Circular microwave tomographic imaging. Experimental comparison between quantitative and qualitative algorithms

Circular Microwave Tomographic Imaging. Experimental Comparison between Quantitative and Qualitative Algorithms

M. Guardiola*, A. Fhager†, L. Jofre*, M. Persson†
*AntennaLab, Universitat Politècnica de Catalunya, Jordi Girona 1-3, 08034 Barcelona (Spain)
{marta.guardiola, jofre}@tsc.upc.edu
†Department of Signals and Systems, Chalmers University of Technology, SE-412 96 Göteborg (Sweden)
andreas.fhager@chalmers.se

***Abstract*—The iterative Time Domain Inversion tomographic algorithm (TDI) proposed by Chalmers University of Technology is compared in terms of image quality to the UWB Magnitude Combined tomographic algorithm (MC-UWB) proposed by the Universitat Politècnica de Catalunya (UPC). The first is able to provide quantitative permittivity images of the object under test, while the second provides quantitative images, being its major strength the short reconstruction time (real time) and robustness. The comparison between the algorithms will be performed based on experimental measurements acquired with two tomographic setups, available at both universities. The Chalmers setup provides a short acquisition time but a narrow band behavior due to the monopole antennas, while the UPC setup is slower but uses broadband antennas.**

I. Introduction

In the framework of microwave tomography, during the last years, different algorithms and experimental systems have been developed for imaging of embedded or complex objects, especially in the medical diagnosis and treatment field. Microwave signals, provide a good compromise between resolution and penetration of biological tissues, which, together with the capability to differentiate features according to their dielectric properties, boosted its application to the well-known breast cancer detection topic [1], and to a lesser extent, to brain stroke or cardiovascular diseases detection [2].

Nowadays there is a growing trend towards developing clinical prototypes to test the algorithms with real patients or tissue-mimicking phantoms in realistic measurement scenarios. The potential of microwave imaging for practical clinical use is significant provided by its low-power non-ionizing radiation, non-contacting application and relatively low-cost system implementation. Among them, cylindrical or circular systems used to be one of the most common geometries of application [1], [3]–[5]. This paper will focus on experimental measurements obtained with a circular array of antennas to study the performance of two different reconstruction algorithms.

When looking at the reconstructed image quality, the main challenge is how to combine a correct geometry reconstruction of the overall structure of the object, including the smaller objects inside it, with an accurate dielectric properties reconstruction.

The goal of this joint paper is to perform a preliminary comparison between the quality of the images (in terms of the two aforementioned features) obtained by a quantitative technique, as the Time Domain Inversion Algorithm [6], with a more qualitative one, as the UWB Magnitude Combined Tomography [7]. The comparison will be performed based on the results obtained with two experimental setups available at Chalmers and UPC, using objects of different shape, size and materials.

The rest of the paper is organized as follows: In next section, the theoretical background of both algorithms will be outlined. Section III is devoted to the comparison of the image quality and performance of both algorithms. Finally the conclusions are drawn in section IV.

II. Imaging Algorithms

Active microwave imaging methods rely on recovering the dielectric properties of an object under test from the scattered fields measured from a number of antennas distributed around it. To do so, a microwave signal is transmitted from one antenna and the scattered signals are received at the remaining antennas of the array. This process is successively repeated until all the antennas have been used as transmitters.

Among the existing imaging algorithms, one can distinguish between radar-based or tomographic methods. Even when common aspects in terms of wave propagation may be found, some conceptual differences exist. While the first one obtains a qualitative image (in terms of dielectric properties) of the most significant scatterers in the reconstruction area, tomographic methods can provide a quantitative complex permittivity image by solving the corresponding inverse scattering problem. Focusing in tomographic techniques, iterative algorithms and diffraction tomography are the most recurrent approaches. This paper compares two tomographic algorithms: Time Domain Inversion algorithm (Chalmers), which falls in the iterative techniques area, and UWB Magnitude Combined Tomographic algorithm (UPC), which is partially based on diffraction tomography. In principle, it is well-known that

diffraction tomography methods can provide a computationally efficient quantitative reconstruction for electrically small or low-contrast objects, producing residual frequency dependent phase errors when the hypothesis of negligible scattered field cannot be assumed. When this occurs, which is often the case in medical imaging applications, more computationally demanding iterative methods need to be used, or instead some compensating mechanism, as the one proposed in the MC-UWB method.

A. Time Domain Inversion Algorithm

The Time Domain Inversion Algorithm is based on minimizing a cost function F containing the difference between the measured data and the corresponding numerical simulation via a conjugate-gradient optimization scheme:

$$F(\epsilon,\sigma)=\int_0^T\sum_{i=1}^{N_T}\sum_{j=1}^{N_R}(|E^s(\epsilon,\sigma,\vec{r}\,'_{R_j},t,\vec{r}\,'_{T_i})- E^m(\vec{r}\,'_{R_j},t,\vec{r}\,'_{T_i})|^2)dt \quad (1)$$

where ϵ and σ are the reconstructed permittivity and conductivity profiles of the target, $E^s(\epsilon,\sigma,\vec{r}\,'_{R_j},t,\vec{r}\,'_{T_i})$ is the simulated field from the FDTD computational model of the setup and $E^m(\vec{r}\,'_{R_j},t,\vec{r}\,'_{T_i})$ is the measured field. N_T and N_R are the number of transmitters and receivers respectively, and $\vec{r}\,'_{T_i}$ refers to the position of the transmitting element and $\vec{r}\,'_{R_j}$ to the position of the receiving element, as shown in Fig. 1.

In the reconstruction procedure, an initial dielectric distribution is assumed in order to compute the first field distribution, E^s. If no *a priori* information of the targets is available, it is set equal to a uniform background. In each iteration, the gradients are derived considering a small increment in the permittivity and conductivity profile, and the corresponding change in the functional is derived by means of a perturbation analysis, [8]. Once the gradients have been updated, the optimization condition is evaluated. Successively improved images are obtained and the process is iterated until the convergence of the cost functional is reached.

From the implementation point of view, the reconstructions presented in the following section are obtained using Gaussian pulses (center frequency of 0.5 GHz and FWHM of 0.5 GHz). 10 iterations on a grid of 4 mm followed by 10 additional iterations on a grid of 2 mm are required to obtain the reconstruction. The choice of the frequency range responses to several features which are common in all reconstruction algorithms, such as the trade-off between increasing the frequency to improve the resolution, and decreasing it to enhance the penetration, and others which depend on the algorithm own requirements. In the case of TDI algorithm, an illumination frequency too high can lead to problems when imaging large structures and high-contrast objects due to the intensification of the nonlinearities.

B. Circular UWB Magnitude Combined Tomography

The UWB Magnitude Combined algorithm, as the name suggests, proposes a compound coherent multiview image addition, which is typical of the diffraction tomography based algorithms, followed with a magnitude multifrequency image combination in the last step of the algorithm. MC-UWB obtains the contrast spectrum of the target, defined as $C(\vec{r})=1-\frac{\epsilon(\vec{r})}{\epsilon_{ext}}$, sampled along a circumference of radius $k_{0,ext}$ centered at $-k_{0,ext}\hat{r}_T$, [9]:

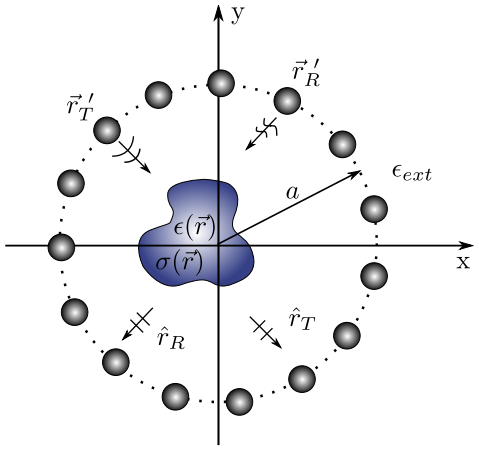

Fig. 1. The object under test of permittivity $\epsilon(\vec{r})$ and conductivity $\sigma(\vec{r})$ is immersed in a medium of permittivity ϵ_{ext}. The circular array of antennas of radius a is composed by $N_T=N_R$ transmitters and receivers. $\vec{r}\,'_{T,R}$ refers to the position of the transmitting and receiving antennas respectively and $\hat{r}_{T,R}$ is the direction of the plane wave.

$$\tilde{C}(k_{0,ext}(\hat{r}_R+\hat{r}_T))=\frac{a^2}{j2\pi f_0\epsilon_{ext}}\sum_{i=1}^{N_T}\sum_{j=1}^{N_R}E^m(\vec{r}\,'_{R_j},f_0;\vec{r}\,'_{T_i}) I(\vec{r}\,'_{R_j},f_0;\hat{r}_R)I(\vec{r}\,'_{T_i},f_0;\hat{r}_T) \quad (2)$$

being $k_{0,ext}=2\pi f_0\sqrt{\mu_{ext}\epsilon_{ext}}$ the wavenumber in the background medium, f_0 is the illuminating frequency and ϵ_{ext} is the permittivity of the background. $I(\vec{r}\,'_{T_i},f_0;\hat{r}_T)$ and $I(\vec{r}\,'_{R_j},f_0;\hat{r}_R)$ are the amplitude coefficients to be applied to each probe of the transmitting or receiving array of radius a to synthesize a plane wave directed to $\hat{r}_T$ or $\hat{r}_R$ respectively.

For highly contrasted objects, where the illuminating field distribution inside the object is not the same for the different transmitters, one can interpret this multiview combination as a way to create a uniform equivalent illuminating field inside the object. The proposed frequency addition technique, takes advantage of the increasing spatial resolution and robustness of a multifrequency combination by using only the amplitude of the images to avoid the speakle produced by the non-linear frequency dependent phase errors. When the phase information is neglected, quantitative permittivity values cannot be recovered. Instead, MC-UWB images present the contrast in permittivities, which is likewise useful to differentiate tissues.

From a practical point of view, the algorithm combines a number of images obtained at different frequencies ranging from 0.1 GHz to 1 GHz. In the case of MC-UWB algorithm, the frequency band of illumination is bounded to avoid aliasing for a given number of antennas.

III. Experimental Results

Two different imaging setups are considered in this section. The system of Chalmers has the advantage of having a switched real array of antennas which reduces substantially the measurement time while avoids disturbances due to the antenna movements. On the other hand, the system of UPC has a only a transmitting and a receiving antenna which are rotated independently and concentrically to virtually obtain a circular array for each one, being its major strength the broadband characteristic of the antennas.

Two different sets of measurements are taken for each reconstruction: one acts as a reference and is taken in absence of the object under test (empty), and the other one with the presence of the object (full).

A. Imaging setup at Chalmers

The experimental system of Chalmers is shown in Fig. 2. It consists of a circular array of $N_T = N_R = 20$ identical monopole antennas evenly distributed on a $a = 200$ mm-diameter circle and mounted on a ground plane inside a tank. The measurements are made in deionized water ($\epsilon_{ext} = 77 + j0.9$ at 1 GHz). A network analyzer (PNA) is used to measure the transmission and reflection coefficients at a large number of discrete frequencies between 0.1 - 4 GHz. To be able to control the measurement sequence, a 2:32 switch multiplexer module was used to automatically connect and disconnect the transmitting and receiving antennas to the PNA.

(a) (b)

Fig. 2. (a) Photograph of the experimental setup of Chalmers. (b) Detail of the antenna array inside the measurement tank.

With this setup, two different scenarios are investigated. The first consists of a cylindrical plastic container filled with a mixture of deionized water and ethanol ($\epsilon = 55 + j7.6$ at 1 GHz) situated at $(80, 118)$ mm, see Fig. 3. The second scenario, see Fig. 4, contains a centered target which is the same as in the previous scenario and a plastic rod situated at $(80, 130)$ mm.

Once these scenarios have been reconstructed with the two imaging algorithms, see Fig. 3 and Fig. 4, it can be seen that both are able to retrieve a successful result in terms of geometry reconstruction. In terms of dielectric properties reconstruction, MC-UWB method presents the contrast in dielectric permittivities normalized and in dB scale, and the TDI algorithm recovers successfully the permittivity values, although presents a bigger error in the conductivity.

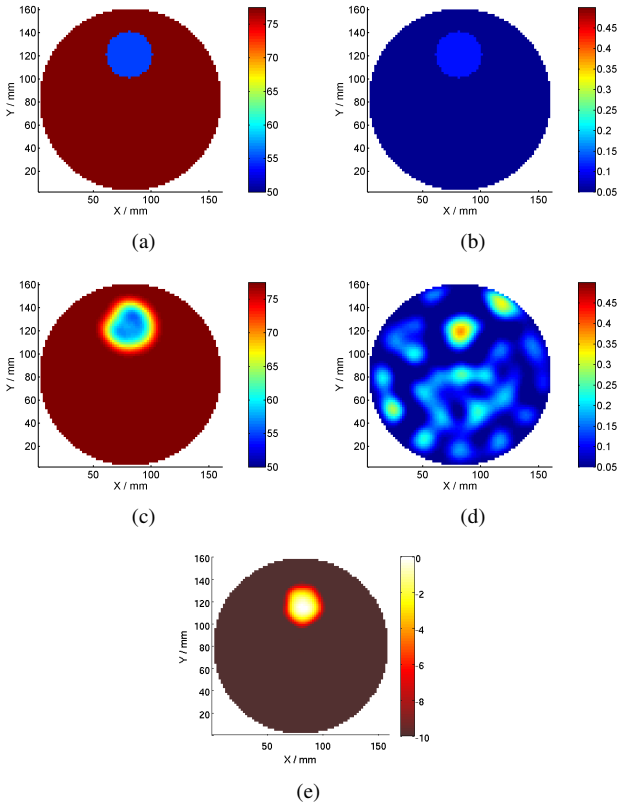

Fig. 3. Reconstructions of a deionized water/ethanol mixture contained in a plastic container. (a) Original permittivity, (b) Original conductivity, (c) Reconstruction of the permittivity with TDI, (d) Reconstruction of the conductivity with TDI, (e) Reconstruction of the contrast using MC-UWB.

B. Imaging setup at UPC

The experimental setup of UPC, Fig. 5, consists of a rotatory distilled water container where the object under test is immersed. Two UWB planar elliptical monopoles fed by coplanar waveguide are used as transmitting and receiving antennas. The transmitter is in a fixed position while the receiver rotates jointly with another rotary stage situated upside down on the top of the setup. The combined rotation of all the elements synthesize two circular virtual arrays of $N_T = N_R = 64$ antennas with diameters $a_T = 270$ mm and $a_R = 200$ mm for the transmitter and the receiver respectively. A network analyzer (PNA) is used to measure the transmission and reflection coefficients between 0.1 - 1 GHz. A computer allows to control remotely the measurement acquisition and the positioning system.

With this setup, two different scenarios are studied. The first one consists of a metallic cylinder of 50 mm diameter and a metallic prism of 40 mm side situated at $(108, 108)$ mm and $(45, 45)$ mm respectively, as shows Fig. 6. The second scenario includes two PVC cylinders of 16 mm diameter situated at $(30, 100)$ mm and $(110, 75)$ mm, see Fig. 7. The reconstructions presented in this part are obtained using MC-UWB algorithm. In both reconstructions a central artifact appears due to differences between the empty and the full

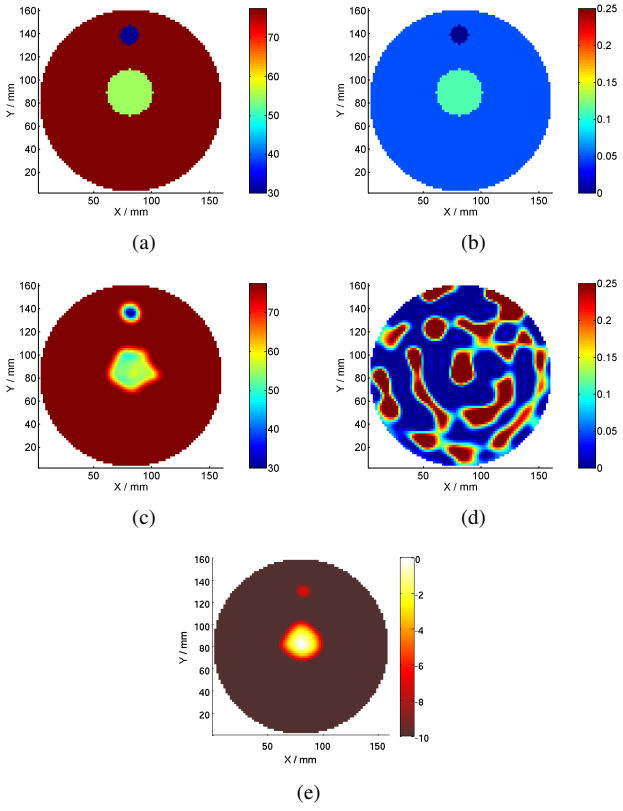

Fig. 4. Reconstructions of a deionized water/ethanol mixture contained in a plastic container and a thinner plastic rod. (a) Original permittivity, (b) Original conductivity, (c) Reconstruction of the permittivity with TDI, (d) Reconstruction of the conductivity with TDI, (e) Reconstruction of the contrast using MC-UWB.

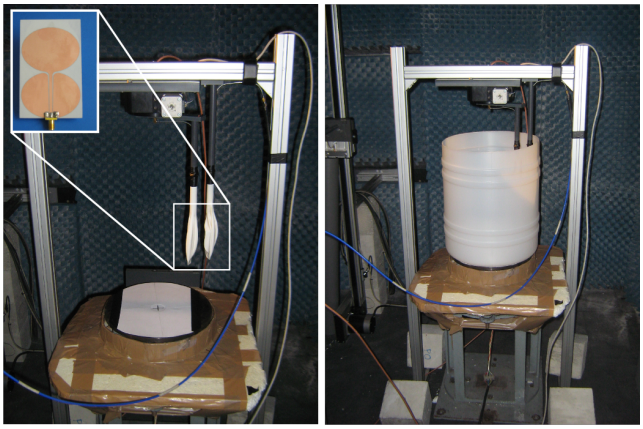

Fig. 5. Photograph of the experimental setup available at UPC

measurement sets which can not be only attributed to the object under test and may be produced by the movement of the setup during the acquisition time. With that in mind, it can be said that the geometrical reconstruction is satisfactory since the shape, size and position of the objects are well reconstructed.

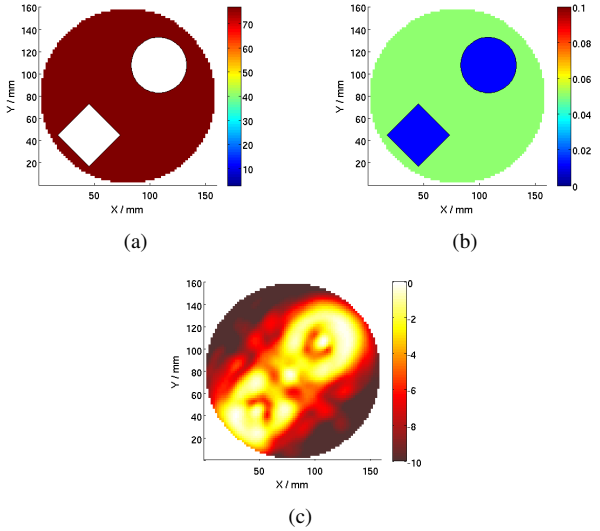

Fig. 6. Reconstruction of a metallic cylinder and a metallic prism. (a) Original permittivity, (b) Original conductivity, (c) Reconstruction of the contrast using MC-UWB.

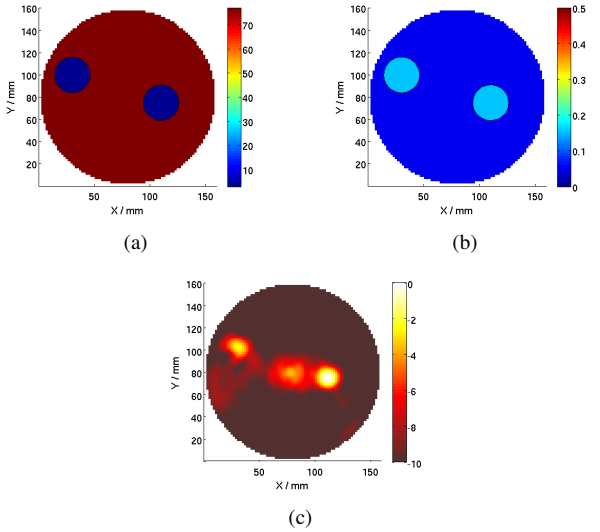

Fig. 7. Reconstruction of 2 PVC rods. (a) Original permittivity, (b) Original conductivity, (c) Reconstruction of the contrast using MC-UWB.

IV. Conclusions

In this paper an initial comparison between the iterative Time Domain Inverse algorithm and the UWB Magnitude Combined method is performed based on experimental measurements. Both algorithms are able to successfuly retrieve a geometrical reconstruction providing the shape, position and size of the objects. In terms of dielectric properties reconstruction, the behavior of each algorithm is different. While the Time Domain Inverse algorithm is able to obtain a quantitative permittivity reconstruction, MC-UWB allows to differentiate tissues or objects based on the contrast in permittivities between them. Accordingly, the Time Domain Inversion technique can provide a more detailed information of the object under test at expenses of a higher reconstruction

time. On the other hand, MC-UWB is capable to provide a qualitative reconstruction in a robust and efficient way (real time) minimizing the required information about the setup.

ACKNOWLEDGMENT

This work was supported in part by the Spanish Inter-ministerial Commission on Science and Technology (CICYT) under projects TEC2010-20841-C04-02 and CONSOLIDER CSD2008-00068, by Ministerio de Educación y Ciencia through the FPU fellowship program, by VINNOVA within the VINN Excellence Center Chase, and by SSF within the Strategic Research Center Charmant.

REFERENCES

[1] P. Meaney, M. Fanning, D. Li, S. Poplack, and K. Paulsen, "A clinical prototype for active microwave imaging of the breast," *Microwave Theory and Techniques, IEEE Transactions on*, vol. 48, no. 11, pp. 1841 – 1853, Nov. 2000.

[2] S. Semenov, R. Svenson, V. Posukh, A. Nazarov, Y. Sizov, A. Bulyshev, A. Souvorov, W. Chen, J. Kasell, and G. Tatsis, "Dielectrical spectroscopy of canine myocardium during acute ischemia and hypoxia at frequency spectrum from 100 khz to 6 ghz," *Medical Imaging, IEEE Transactions on*, vol. 21, no. 6, pp. 703 –707, 2002.

[3] M. Guardiola, L. Jofre, S. Capdevila, S. Blanch, and J. Romeu, "Toward 3d uwb tomographie imaging system for breast tumor detection," in *Antennas and Propagation (EuCAP), 2010 Proceedings of the Fourth European Conference on*, 2010, pp. 1 –5.

[4] L. Jofre, M. Hawley, A. Broquetas, E. de los Reyes, M. Ferrando, and A. Elias-Fuste, "Medical imaging with a microwave tomographic scanner," *Biomedical Engineering, IEEE Transactions on*, vol. 37, no. 3, pp. 303 –312, 1990.

[5] S. Semenov, R. Svenson, A. Souvorov, A. Bulyshev, A. Nazarov, Y. Sizov, A. Pavlovsky, V. Posukh, and G. Tatsis, "Microwave tomography. experimental imaging on two and three dimensional systems," in *Microwave Symposium Digest, 1998 IEEE MTT-S International*, vol. 2, June 1998, pp. 763 –765 vol.2.

[6] A. Fhager, P. Hashemzadeh, and M. Persson, "Reconstruction quality and spectral content of an electromagnetic time-domain inversion algorithm," *Biomedical Engineering, IEEE Transactions on*, vol. 53, no. 8, pp. 1594 –1604, 2006.

[7] M. Guardiola, S. Capdevila, S. Blanch, J. Romeu, and L. Jofre, "Uwb high-contrast robust tomographic imaging for medical applications," in *Electromagnetics in Advanced Applications, 2009. ICEAA '09. International Conference on*, Sept. 2009, pp. 560–563.

[8] M. Gustafsson and S. He, "An optimization apporach to two-dimensional time domain electromagnetic inverse problems," *Radio Sci.*, vol. 35, pp. 525–536, 2000.

[9] J. Rius, C. Pichot, L. Jofre, J. Bolomey, N. Joachimowicz, A. Broquetas, and M. Ferrando, "Planar and cylindrical active microwave temperature imaging: numerical simulations," *Medical Imaging, IEEE Transactions on*, vol. 11, no. 4, pp. 457–469, Dec 1992.